2021

A strongly Lewis-acidic and fluorescent borenium cation supported by a tridentate formazanate ligand

Benjamin D. Katzman

Ryan R. Maar

Daniela Cappello

Madeleine O. Sattler

Paul D. Boyle

See next page for additional authors

COMMUNICATION

A strongly Lewis-acidic and fluorescent borenium cation supported by a tridentate formazanate ligand

Received 00th January 20xx,
Accepted 00th January 20xx

DOI: 10.1039/x0xx00000x

Benjamin D. Katzman,[a] Ryan R. Maar,[a] Daniela Cappello,[a] Madeleine O. Sattler,[a] Paul D. Boyle,[a] Viktor N. Staroverov,[a] and Joe B. Gilroy[a*]

Lewis acids are highly sought after for their applications in sensing, small-molecule activation, and catalysis. When combined with π-conjugated molecular frameworks, Lewis acids with unique optoelectronic properties can be realized. Here, we use a tridentate formazanate ligand to create a planar, redox-active, fluorescent, and strongly Lewis-acidic borenium cation. We also demonstrate that this compound can act as a colourimetric probe for reactivity.

The Lewis acid-base theory is one of the most important fundamental concepts that have shaped our modern understanding of chemical reactivity, structure, and bonding. The search for new Lewis acids is often motivated by their applications in areas such as bond and small-molecule activation and catalysis.[1-4] As a result, a wide variety of Lewis acids based on main-group elements have been reported (Fig. 1). Perhaps counterintuitively, these examples include not only elements of group 13 but also atoms with more than three valence electrons: for example, nitrogen (**1**),[5,6] phosphorus (**2**),[7,8] and silicon (**3**).[9,10] However, electron-deficient compounds based on group-13 elements remain the most characteristic types of Lewis acids, with neutral (*e.g.*, **4**)[11-12,13-17] and cationic (*e.g.*, **5**)[11, 18,19-23] boron compounds being especially common. Such Lewis acids have shown promise as structural components of functional materials when incorporated into π-conjugated scaffolds[24-25] with applications as sensors.[26,27-28]

Formazanate ligands[29] (**6**) are an emerging class of π-conjugated ligands that afford unusual optoelectronic properties when combined with transition metals and main-group elements. Examples of their use include homoleptic Fe complexes with atypical spin crossover characteristics that are controlled by varying the electronic properties of supporting formazanate ligands,[30-31] BF_2 adducts that exhibit near-IR fluorescence and electrochemiluminescence leading to their application as cancer theranostics,[32-33] and hypercoordinate group 14 complexes of formazanate ligands that act as precursors to stable radicals in the absence of significant steric bulk.[34] Very recently, it was demonstrated that the optoelectronic properties of mono- and dicationic boron complexes of a bidentate formazanate ligand can be modulated by varying the charge, coordination number, and identity of the supporting ligands at boron.[35]

In this work, we execute a design strategy based on a novel tridentate formazanate ligand to create a planar borenium complex that is strongly Lewis-acidic and fluorescent. Proof-of-concept reactions with an F^- source demonstrate the promise of this new borenium cation as a colourimetric reactivity probe.

Formazan **7** was prepared in 43% yield as a red solid by the coupling reaction between 1-(*p*-tolyl)-3-phenylhydrazone and 2-(hydroxybenzene)diazonium chloride in the presence of NaOH and NaOAc in MeOH (Scheme S1, Fig. S1 and S2, ESI†). Formazan **7** has a diagnostic NH resonance at 14.95 ppm in its ^{1}H NMR spectrum in DMSO-*d6*. The BF formazanate adduct **8** was generated by heating a solution of formazan **7**, NEt_3, and $BF_3{\bullet}OEt_2$ in toluene at 120 °C for 48 h (Scheme 1, Fig. S3–S6, ESI†). After purification by column chromatography, BF formazanate **8** was isolated as a dark purple solid in 61% yield. Its ^{1}H NMR spectrum lacked the NH resonance previously

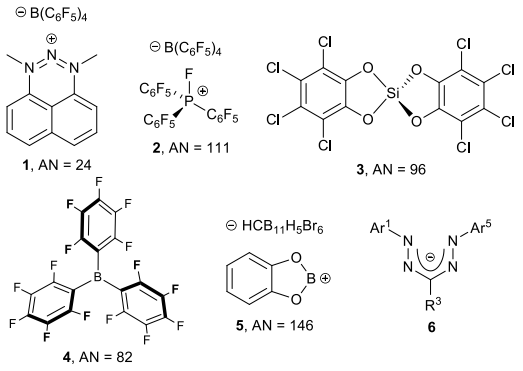

Fig. 1 Chemical structures for Lewis acids **1**–**5** based on various main-group elements. Gutmann-Beckett acceptor numbers (AN)[36-37] are provided for comparison. Also shown is the structure of a formazanate ligand **6**.

[a] *Department of Chemistry and the Centre for Advanced Materials and Biomaterials Research (CAMBR), The University of Western Ontario, London, Ontario, Canada.*

†Electronic Supplementary Information (ESI) available: [X-ray diffraction methods, synthetic procedures, copies of NMR spectra, computational methods, and molecular coordinates]. See DOI: 10.1039/x0xx00000x

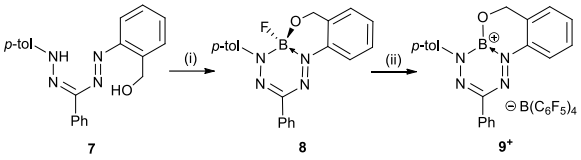

Scheme 1 Synthesis of BF formazanate **8** and borenium cation **9**$^+$; (i) = NEt_3, BF_3•OEt_2, toluene, 120 °C, 48 h; (ii) = $[Et_3Si(C_7H_8)][B(C_6F_5)_4]$, toluene, 22 °C, 1h.

observed for formazan **7**, but showed two doublets at 5.27 and 4.82 ppm due to the diastereotopic CH_2 group and new $^{11}B\{^1H\}$ (–0.8 ppm, d, $^1J_{BF}$ = 38 Hz) and $^{19}F\{^1H\}$ (–156.1 ppm, q, $^1J_{FB}$ = 38 Hz) NMR resonances in the respective spectra. The conversion of BF formazanate **8** to borenium cation **9**$^+$ was accomplished by the abstraction of F^- using $[Et_3Si(C_7H_8)][B(C_6F_5)_4]$[38] (Scheme 1, Fig. S7–S10, ESI†). Cation **9**$^+$ was isolated in 87% yield as a dark green microcrystalline solid. Borenium cation **9**$^+$ gave a singlet at 5.86 ppm due to its CH_2 group in the ^1H NMR spectrum as well as singlets at 21.2 and –16.8 ppm in the ^{11}B NMR spectrum corresponding to the three-coordinate (borenium) cation and the $B(C_6F_5)_4^-$ anion, respectively. The ^{19}F NMR spectrum of cation **9**$^+$ was comprised of three signals between –133.2 and –167.7 ppm corresponding to the $B(C_6F_5)_4^-$ anion. Unlike BF formazanate **8**, borenium cation **9**$^+$ is moisture-sensitive and generally unstable in the presence of Lewis bases.

The molecular and electronic structures of BN heterocycles **8** and **9**$^+$ differ dramatically due to the four-coordinate neutral and three-coordinate cationic boron atoms they contain. The solid-state structures of compounds **8** and **9**$^+$ (Fig. 2, Table S1 and S2, ESI†) determined by single-crystal X-ray diffraction demonstrate that the formazanate (N1-N2-C1-N3-N4) π system is delocalized in both compounds, with average N-N [**8**: 1.3119(14) Å; **9**$^+$: 1.323(2) Å] and N-C [**8**: 1.3436(16) Å; **9**$^+$: 1.339(2) Å] bond lengths. The boron atom lies 0.6190(19) Å above the plane defined by N1-N2-N3-N4 in BF formazanate **8** and 0.056(3) Å above a similarly defined plane in borenium cation **9**$^+$. Borenium cation **9**$^+$ has a flatter CN_4B ring and shorter average B-N bonds [1.456(3) Å] than BF formazanate **8** [1.5676(17) Å].

The molecular geometries of **8** and **9**$^+$ in CH_2Cl_2 solution calculated using density-functional theory (DFT) with the TPSSh/def2-TZVP method (see computational details in the Supplementary Information) were similar to the solid-state structures obtained experimentally. The frontier orbitals reveal subtle but important differences between the two compounds (Fig. 2). The highest occupied molecular orbitals (HOMOs) are of π-type and are fully delocalized over the entire molecule in each of compounds **8** and **9**$^+$. However, the flatter structure of borenium cation **9**$^+$ affords a greater degree of delocalization through the boron atom and permits a higher degree of p-π orbital overlap. The π* type lowest unoccupied molecular orbitals (LUMOs) are primarily located on the formazanate ligand with limited contributions from the boron atoms.

The changes in molecular and electronic structure as well as the observed differences in the colour of compounds **8** and **9**$^+$

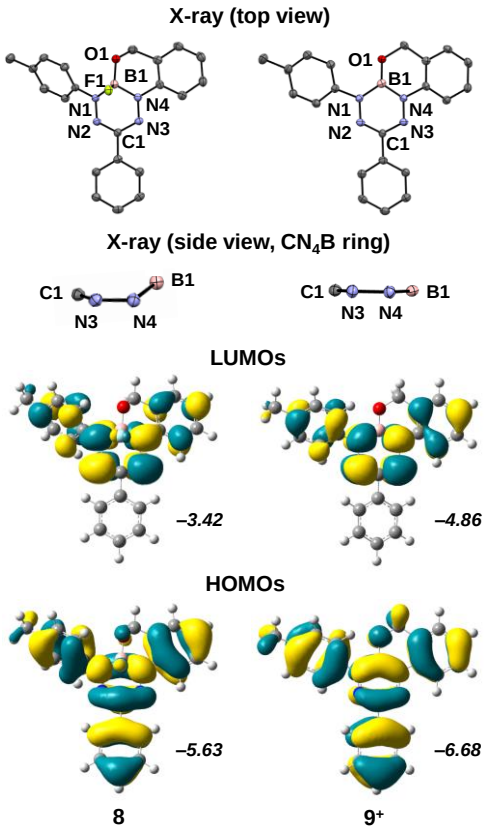

Fig. 2 Solid-state structures of BF formazanate **8** and borenium cation **9**$^+$ (anisotropic displacement ellipsoids at 50% probability; hydrogen atoms, solvent molecules, and counter-anions are omitted for clarity); frontier molecular orbitals and their energies (in eV) calculated using the TPSSh/def2-TZVP method for BF formazanate **8** and borenium cation **9**$^+$ solvated by CH_2Cl_2.

prompted us to explore their electronic properties using UV-vis absorption and emission spectroscopy, time-dependent DFT (TDDFT), and cyclic voltammetry (CV). In CH_2Cl_2 solution, BF formazanate **8** exhibited a broad low-energy absorption band centred at λ_{abs}^{exp} = 530 nm (ε = 20,200 M^{-1} cm^{-1}) which is comparable to that of related BF_2 formazanate dyes (Fig. 3a).[39] Under similar conditions, borenium cation **9**$^+$ showed a red-shifted absorption band with vibrational fine structure due to its planar and rigid structure at λ_{abs}^{exp} = 650 nm (ε = 8,000 M^{-1} cm^{-1}). In both cases, TDDFT at the TPSSh/def2-TZVP level predicted matching lowest-energy excitations with the HOMO and LUMO as the dominant orbital pairs involved [**8**: λ_{abs}^{calc} = 527 nm (f = 0.393); **9**$^+$: λ_{abs}^{calc} = 663 nm (f = 0.224)]. DFT calculations also demonstrate that the HOMO-LUMO gap in borenium cation **9**$^+$ is smaller than in BF formazanate **8** (Fig. 2), which is consistent with the relative positions of the lowest-energy absorption peaks of **9**$^+$ and **8** in their experimental UV-vis absorption spectra (Fig. 3). BF formazanate **8** was non-emissive in solution, while borenium cation **9**$^+$ exhibited strong fluorescence (λ_{em}^{exp} = 672 nm, ϕ_F = 0.38) as a result of its nearly planar, conjugated structure. The relatively narrow emission band observed for borenium cation **9**$^+$ was the result of the secondary inner-filter effect and the relatively small Stokes shift

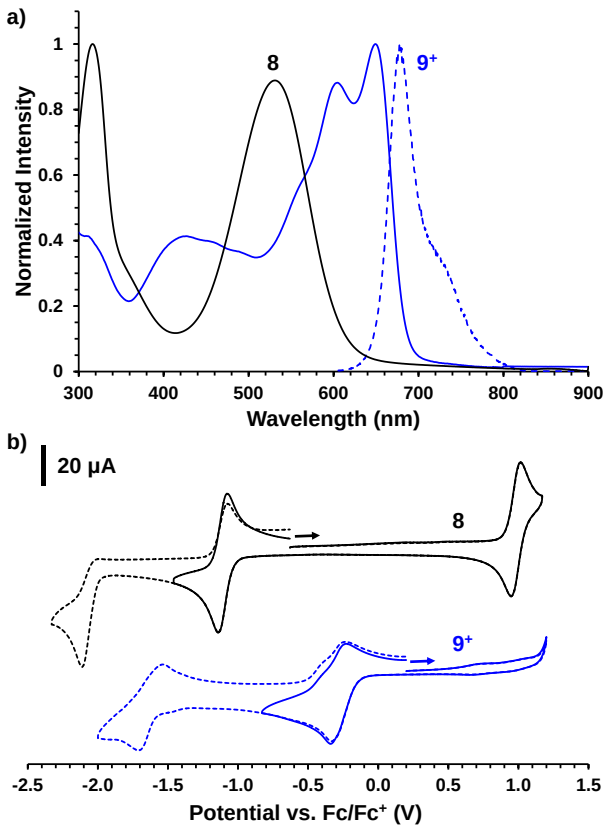

Fig. 3 a) UV-vis absorption (solid lines) and emission (dashed line) spectra recorded for BF formazanate **8** and borenium cation **9**$^+$ in dry, degassed CH_2Cl_2. b) Cyclic voltammograms recorded for 0.1 mM solutions of BF formazanate **8** and borenium cation **9**$^+$ in CH_2Cl_2 containing 0.1M [nBu$_4$N][B(C$_6$F$_5$)$_4$] as supporting electrolyte. The scan rate was 250 mV s^{-1}. The arrows denote the initial scan direction.

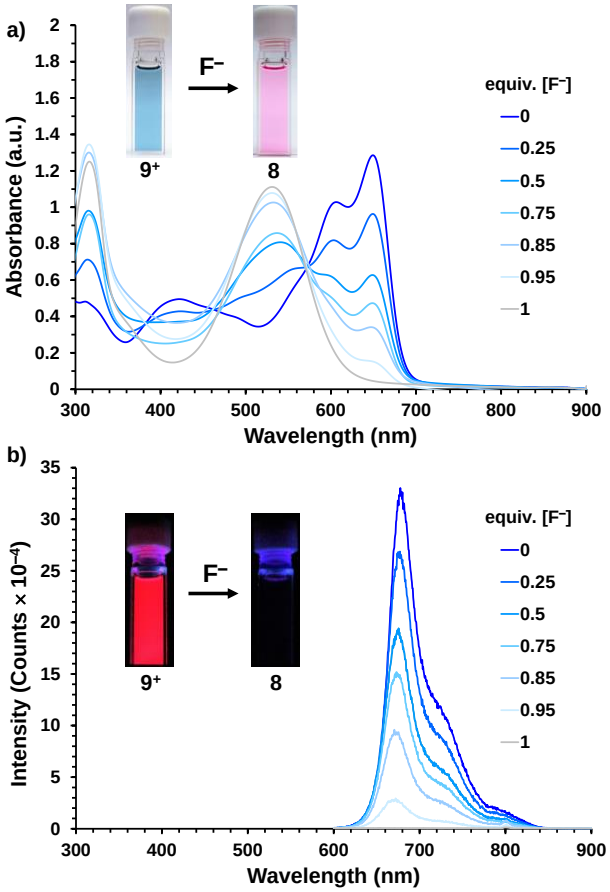

Fig. 4 UV-vis a) absorption and b) emission spectra collected for 80 µM solutions of borenium cation **9**$^+$ in dry and degassed CH_2Cl_2 upon mixing with varying quantities of [nBu$_4$N][SiPh$_3$F$_2$]. Photographs of 80 µM solutions taken in ambient light (top) and under long-wave UV irradiation (bottom).

(ν_{ST} = 22 nm, 504 cm^{-1}) observed as a consequence of the structural rigidity imparted by the tridentate formazanate ligand.

The relatively low LUMO energy of borenium cation **9**$^+$ prompted us to examine the electrochemical properties of compounds **8** and **9**$^+$ using cyclic voltammetry (Fig. 3b). The CV of compound **8** revealed a reversible one-electron oxidation wave (**8** → **8**$^{\bullet+}$) centred at 0.97 V (relative to the ferrocene/ferrocenium redox couple) as well as reversible (**8** → **8**$^{\bullet-}$) and irreversible (**8**$^{\bullet-}$ → **8**$^{2-}$) one-electron reduction waves at –1.12 V and –2.12 V (potential at peak cathodic potential). No oxidation for borenium cation **9**$^+$ was observed within the solvent stability window. However, two reversible one-electron reduction waves corresponding to the electrochemical generation of neutral radical **9**$^\bullet$ and anion **9**$^-$ were observed at of –0.30 V and –1.62 V. Using the equation $E_{LUMO}^{CV} = -4.8 - E_{onset}^{red}$,[40] we estimate the LUMO energies for **8** and **9**$^+$ to be –3.77 eV (E_{LUMO}^{DFT} = –3.42 eV) and –4.70 eV (E_{LUMO}^{DFT} = –4.86 eV), respectively.

Compounds with low-lying LUMO orbitals and planar structures are often excellent Lewis acids.[41] When borenium cation **9**$^+$ was combined with a stoichiometric equivalent of OPEt$_3$, the resulting Lewis acid-base adduct (**9**$^+$•OPEt$_3$) gave an ^{11}B{^{1}H} NMR signal at –0.9 ppm (Fig. S11 and S12, ESI†). This confirms the formation of a four-coordinate boron centre upon coordination of OPEt$_3$, possibly through the interaction with the LUMO+1 of cation **9**$^+$ (Fig. S13, ESI†). The ^{31}P{^{1}H} NMR chemical shift of **9**$^+$•OPEt$_3$ is 86.7 ppm in CD_2Cl_2 (Fig. S11, ESI†). This corresponds to an exceptionally high Gutmann-Beckett AN of 101. For comparison, the now ubiquitous Lewis acid B(C$_6$F$_5$)$_3$ (**4**) has AN = 82 under similar conditions.[13] Motivated by the work of Jäkle and co-workers,[42] we also conducted a competition experiment by mixing **9**$^+$, B(C$_6$F$_5$)$_3$, and OPEt$_3$ in a 1:1:0.95 ratio in CD_2Cl_2 (Fig. S12, ESI†). Under these conditions, integration of the ^{31}P{^{1}H} NMR signals associated with **9**$^+$•OPEt$_3$ and B(C$_6$F$_5$)$_3$•OPEt$_3$ revealed the existence of these adducts in a 1:0.8 ratio. These data further confirm the strong Lewis acidity of borenium cation **9**$^+$.

The extreme Lewis acidity and attractive optoelectronic properties of **9**$^+$ make this borenium cation a strong candidate for use as a colourimetric reactivity probe in the realms of Lewis acid catalysis and sensing. To demonstrate this concept, we monitored both UV-vis absorption and emission channels of 80 µM solutions of borenium cation **9**$^+$ in CH_2Cl_2 containing different molar equivalents of [nBu$_4$N][SiPh$_3$F$_2$]. Under these conditions, **9**$^+$ abstracts F$^-$ from [nBu$_4$N][SiPh$_3$F$_2$]. The corresponding absorption spectra reveal the stepwise disappearance of the low-energy absorption band associated

with borenium cation **9**$^+$ (λ_{abs}^{exp} = 650 nm) and the appearance of an absorption band for BF formazanate **8** (λ_{abs}^{exp} = 530 nm). Similarly, the fluorescence intensity of solutions of borenium cation **9**$^+$ exhibits a near-linear turn-off response when **9**$^+$ abstracted F^- from [*n*Bu_4N][$SiPh_3F_2$].

In conclusion, we have demonstrated that one can impart boron formazanate complexes with useful optoelectronic properties by switching between four-coordinate neutral and three-coordinate cationic boron environments, as in compounds **8** and **9**$^+$. Most notably, borenium cation **9**$^+$ [λ_{abs}^{exp} = 650 nm (ε = 8,000 M^{-1} cm^{-1}); λ_{em}^{exp} = 672 nm (ϕ_F = 0.38); E_{LUMO}^{CV} = –4.70 eV] exhibits a lower energy absorption maximum and intense fluorescence as a result of ligand-enforced planarity and rigidity, and a stabilized LUMO when compared to BF formazanate **8** [λ_{abs}^{exp} = 530 nm (ε = 20,200 M^{-1} cm^{-1}); non-emissive; E_{LUMO}^{CV} = –3.77 eV]. The low-lying LUMO of borenium cation **9**$^+$ is responsible for the strong Lewis acidity (AN = 101). As a proof of concept, we also demonstrated that the unique optoelectronic properties of **9**$^+$ and its remarkable Lewis acidity enable this cationic complex to serve as a colourimetric probe (via both absorption and emission) of Lewis acid-base reactivity. Future work in this area will investigate the scope and efficacy of such probes in the small-molecule activation, catalysis, and sensing arenas.

We gratefully acknowledge financial support from the Natural Sciences and Engineering Research Council (NSERC) of Canada (V.N.S.: DG, RGPIN-2020-06420; J.B.G.: DG, RGPIN-2018-04240, B.D.K.: CGS-M Scholarship, R.R.M. and D.C.: CGS-D Scholarships), the Ontario Ministry of Research and Innovation (J.B.G.: ERA, ER-14-10-147), the Canadian Foundation for Innovation (J.B.G.: JELF, 33977), and The University of Western Ontario. We also thank Mr. Jordan N. Bentley and Dr. Chris B. Caputo (York University) for performing elemental analyses.

Conflicts of interest

There are no conflicts to declare.

Notes and references

1 P. Eisenberger and C. M. Crudden, *Dalton Trans.*, 2017, **46**, 4874–4887.
2 C. Weetman and S. Inoue, *ChemCatChem*, 2018, **10**, 4213–4228.
3 J. Lam, K. M. Szkop, E. Mosaferi and D. W. Stephan, *Chem. Soc. Rev.*, 2019, **48**, 3592–3612.
4 J. L. Carden, A. Dasgupta and R. L. Melen, *Chem. Soc. Rev.*, 2020, **49**, 1706–1725.
5 A. Pogoreltsev, Y. Tulchinsky, N. Fridman and M. Gandelman, *J. Am. Chem. Soc.*, 2017, **139**, 4062–4067.
6 M. Mehta and J. M. Goicoechea, *Angew. Chem. Int. Ed.*, 2020, **59**, 2715–2719.
7 J. M. Bayne and D. W. Stephan, *Chem. Soc. Rev.*, 2016, **45**, 765–774.
8 C. B. Caputo, L. J. Hounjet, R. Dobrovetsky and D. W. Stephan, *Science*, 2013, **341**, 1374–1377.
9 J. C. L. Walker, H. F. T. Klare and M. Oestreich, *Nat. Rev. Chem.*, 2020, **4**, 54–62.
10 R. Maskey, M. Schädler, C. Legler and L. Greb, *Angew. Chem. Int. Ed.*, 2018, **57**, 1717–1720.
11 I. B. Sivaev and V. I. Bregadze, *Coord. Chem. Rev.*, 2014, **270–271**, 75–88.
12 E. A. Patrick and W. E. Piers, *Chem. Commun.*, 2020, **56**, 841–853.
13 M. A. Beckett, D. S. Brassington, S. J. Coles and M. B. Hursthouse, *Inorg. Chem. Commun.*, 2000, **3**, 530–533.
14 A. Schnurr, M. Bolte, H.-W. Lerner and M. Wagner, *Eur. J. Inorg. Chem.*, 2012, 112–120.
15 L. A. Körte, J. Schwabedissen, M. Soffner, S. Blomeyer, C. G. Reuter, Y. V. Vishnevskiy, B. Neumann, H.-G. Stammler and N. W. Mitzel, *Angew. Chem. Int. Ed.*, 2017, **56**, 8578–8582.
16 A. Ben Saida, A. Chardon, A. Osi, N. Tumanov, J. Wouters, A. I. Adjieufack, B. Champagne and G. Berionni, *Angew. Chem. Int. Ed.*, 2019, **58**, 16889–16893.
17 C. Stoian, M. Olaru, T. A. Cucuiet, K. T. Kegyes, A. Sava, A. Y. Timoshkin, C. I. Raţ and J. Beckmann, *Chem. Eur. J.*, 2021, **27**, 4327–4331.
18 W. E. Piers, S. C. Bourke and K. D. Conroy, *Angew. Chem. Int. Ed.*, 2005, **44**, 5016—5036.
19 A. Del Grosso, R. G. Pritchard, C. A. Muryn and M. J. Ingleson, *Organometallics*, 2010, **29**, 241–249.
20 Y. Wang, M. Y. Abraham, R. J. Gilliard, D. R. Sexton, P. Wei and G. H. Robinson, *Organometallics*, 2013, **32**, 6639–6642.
21 J. M. Farrell and D. W. Stephan, *Angew. Chem. Int. Ed.*, 2015, **54**, 5214–5217.
22 H.-C. Tseng, C.-T. Shen, K. Matsumoto, D.-N. Shih, Y.-H. Liu, S.-M. Peng, S. Yamaguchi, Y.-F. Lin and C.-W. Chiu, *Organometallics*, 2019, **38**, 4516–4521.
23 Y. Adachi, F. Arai and F. Jäkle, *Chem. Commun.*, 2020, **56**, 5119–5122.
24 S. K. Mellerup and S. Wang, *Trends Chem.*, 2019, **1**, 77–89.
25 X. Yin, J. Liu and F. Jäkle, *Chem. Eur. J.*, 2021, **27**, 2973–2986.
26 E. Galbraith and T. D. James, *Chem. Soc. Rev.*, 2010, **39**, 3831–3842.
27 T. W. Hudnall and F. P. Gabbaï, *Chem. Commun.*, 2008, 4596–4597.
28 M. Ferger, Z. Ban, I. Krošl, S. Tomić, L. Dietrich, S. Lorenzen, F. Rauch, D. Sieh, A. Friedrich, S. Griesbeck, A. Kendel, S. Miljanić, I. Piantanida and T. B. Marder, *Chem. Eur. J.*, 2021, **27**, 5142–5159.
29 J. B. Gilroy and E. Otten, *Chem. Soc. Rev.*, 2020, **49**, 85—113.
30 R. Travieso-Puente, J. O. P. Broekman, M.-C. Chang, S. Demeshko, F. Meyer and E. Otten, *J. Am. Chem. Soc.*, 2016, **138**, 5503–5506.
31 F. Milocco, F. de Vries, I. M. A. Bartels, R. W. A. Havenith, J. Cirera, S. Demeshko, F. Meyer and E. Otten, *J. Am. Chem. Soc.*, 2020, **142**, 20170–20181.
32 R. R. Maar, R. Zhang, D. G. Stephens, Z. F. Ding and J. B. Gilroy, *Angew. Chem. Int. Ed.*, 2019, **58**, 1052–1056.
33 H. Xiang, L. Zhao, L. Yu, H. Chen, C. Wei, Y. Chen and Y. Zhao, *Nat. Commun.*, 2021, **12**, 218.
34 R. R. Maar, S. D. Catingan, V. N. Staroverov and J. B. Gilroy, *Angew. Chem. Int. Ed.*, 2018, **57**, 9870–9874.
35 R. R. Maar, B. D. Katzman, P. D. Boyle, V. N. Staroverov and J. B. Gilroy, *Angew. Chem. Int. Ed.*, 2021, **60**, 5152—5156.
36 V. Gutmann, *Coord. Chem. Rev.*, 1976, **18**, 225–255.
37 M. A. Beckett, G. C. Strickland, J. R. Holland and K. S. Varma, *Polymer*, 1996, **37**, 4629–4631.
38 S. J. Connelly, W. Kaminsky and D. M. Heinekey, *Organometallics*, 2013, **32**, 7478—7481.
39 S. M. Barbon, J. T. Price, P. A. Reinkeluers and J. B. Gilroy, *Inorg. Chem.*, 2014, **53**, 10585–10593.
40 C. M. Cardona, W. Li, A. E. Kaifer, D. Stockdale and G. C. Bazan, *Adv. Mater.*, 2011, **23**, 2367–2371.
41 L. Greb, *Chem. Eur. J.*, 2018, **24**, 17881–17896.
42 J. Chen, R. A. Lalancette and F. Jäkle, *Chem. Commun.*, 2013, **49**, 4893-4895.

